

Full Length Research Paper

Dynamic wave soil structure interaction analysis of a two way asymmetric building system DSSIA-3D

J. L. Wegner, M. M. Yao and S. K. Bhullar*

Department of Mechanical Engineering, University of Victoria, P. O. Box 3055, Victoria, B. C. Canada V8W 3P6

Accepted 13 May, 2009

In this paper structural response to dynamic loading, which is expressed in terms of displacements of the structure, is studied. A two-way asymmetrical multistory building model is subjected to bi-directional harmonic and earthquake loadings. The time histories of the vertically and horizontal displacements and rotation of the roof are obtained using the scaled boundary finite-element method. The program Dynamic Soil-Structure Interaction Analysis which takes into account the soil-structure interaction effects is applied to study two-way asymmetrical buildings. These results are compared with those of symmetrical buildings.

Key words: Dynamic soil structure interaction, scaled boundary finite-element method, displacements, time varying loading.

INTRODUCTION

Characteristics of dynamic response and damage of structures to seismic motion has been a subject of investigation for the last few decades by many researchers and are quite well understood. It is commonly accepted that structures normally respond at their fundamental frequencies and low vibration modes, and damage of a structure to a seismic motion is mainly caused by excessive structural displacement. Thus, displacement related quantities such as storey drift and ductility ratios are usually employed in analysis and design in earthquake engineering to quantify structural damage. Dynamic soil structure interaction (DSSI) effects when loads act directly on the structure (wind loads, moving machinery, traffic on bridges etc.) are basically due to the foundation compliance.

They can be taken into account by using the foundation stiffness matrix. In many other cases dynamic excitation comes from the soil (earthquakes, nearby road or railway traffic, underground explosions etc.). In those cases, the influence of DSSI on the structural response is twofold: first, the excitation due to wave impinging on the structure depends on the soil properties and on the foundation characteristics; second, the response of the structure to the excitation also depends on DSSI effects. Dynamic

soil-structure interaction has been an active area of research, particularly in relation to seismic effects on underground and embedded structures. Many researchers face problems related to infinitely extended media, such as wave propagating problems in water, soil-structure-interaction, fluid-structure-interaction and acoustic wave problems.

Soil-structure interaction (SSI) is an important issue, especially for stiff and massive structures constructed on the relative soft ground, which may alter the dynamic characteristics of the structural response significantly. Thus, the interaction effects should be accounted for in the dynamic analysis of all soil-structure-system, particularly in severe soil conditions. The SSI system has two characteristic differences from the general structural dynamic system. These are the unbounded nature of the soil and the non-linear characteristics of the soil medium. The radiation of the energy towards infinity, leading to the so called radiation damping, is the most prominent characteristic in an unbounded soil, which is not relevant in a bounded medium. Various studies and contributions have appeared in the literature regarding the effects of SSI on the dynamic seismic response of buildings (Ben et al., 2000). Several types of modeling techniques, analytical methods and theoretical formulations have been developed over the past three decades. These include hybrid modeling methods (Tzong et al., 1983), boundary element (Chen and Penzien, 1986), boundary solution (Lu-

*Corresponding author. E-mail: sbhullar@uvic.ca

co, 1974; Wong and Luco, 1976; Wong and Luco, 1985; Liou, 1989), viscous boundary (Lysmer and Kuhlemeyer, 1969; White et al., 1969), transmitting boundary (Werkle, 1986; Tassoulas, 1983), and scaled boundary finite-element method (Song and Wolf, 1998). All of these methods can be classified into two main categories: the direct method and the substructure method (Song and Wolf, 2000). The destruction in 1985 Mexico earthquake focused researchers on soil-structure interaction effects and on the response behavior of such systems (Chopra, 1995). Asymmetrical buildings are more vulnerable to earthquake hazards compared to the buildings with symmetric configuration. The recognition of this sensitivity has led researchers to concentrate their studies on earthquake characteristics, evaluation of the structural parameters and validity of the system models (Kan and Chopra, 1977; Kan and Chopra, 1981; Hejal and Chopra, 1989; Chandler and Duna, 1991; Shakib and Datta, 1993; Paulay, 1997; Myslimaj and Tso, 2002; Shakib and Touhidi, 2002), among others. So far, several researchers have attempted to evaluate the seismic response behavior of torsionally coupled buildings for the linear analysis of three dimensional dynamic soil-structure interactions of asymmetric buildings (Armando and Luis, 2007). The influence of dynamic soil-structure interaction on seismic response is studied in (Shakib and Fuladgar, 2004), selecting a set of reinforced concrete structures with gravitational loads and mechanical properties representative systems designed for earthquake resistance in accordance with current criteria and methods.

A numerical procedure (DSSIA-3D) was formulated for the analysis of three-dimensional dynamic soil-structure in the time domain by Zhang et al., 1999, which can be used in the analyses of 3D dynamic soil-structure interaction as well as in the analysis of wave scattering and diffraction by three-dimensional surface irregularities, and the numerical results obtained, were in good agreement with those given by others. In a later paper, DSSIA-3D (Wegner and Zhang, 2001) was applied to obtain the dynamic response of a spherical cavity, three-dimensional, free vibration of a dam-foundation system. In that study, the numerical results were embedded in full-space, subjected to seismic waves and compared to the analytical solutions, with excellent agreement. In a recent paper Wegner et al., 2005 applied DSSIA-3D to obtain the dynamic response of tall buildings, with multi-level basements, subjected to realistic seismic excitations, including P-, SH-, SV- waves, at various input angles.

The objective of the present study is to apply DSSIA-3D to study dynamic seismic response of two-way asymmetric buildings, with basements, subjected to bidirectional harmonic and earthquake loadings. A novel semi-analytical procedure called the scaled boundary finite-element method, which is actually a combination of advantages of the finite-element and boundary-ele-

ment method, is implemented. The solution procedures of the scaled boundary finite-element equation in displacement and in dynamic stiffness for bounded and unbounded media are discussed in (Song and Wolf, 2000).

SYSTEM MODEL AND FORMULATION

Model

In past years, seismic response of asymmetric structures has been frequently analyzed by means of single storey model, because of their simplicity and low computational cost. In this paper, a two-way asymmetric 15-storey building with one level basement model, as shown in Figure 1 (a) and (b), is studied. The dimensions of the floors are $18 \times 18 \times 0.40 \text{ m}^3$, the heights between floors and ceilings are 3.10 m and the thickness of walls is 20 cm. Each floor is divided into 4 units separated by walls and the material used for the building is concrete. The wall and floor of this super-structure are meshed into 1872 8-node brick elements with 3 DOFs for each node. There are 1534-node interface elements along the soil-structure interface. The excavated soil is meshed into 162 brick elements at the basement. The total nodal nodes of this building model are 3300. The origin of the Cartesian coordinate system at the center of the first level, where the building's centerline intersects the ground surface, as shown in Figure 1(d). The Z-axis is pointing downward into the half space. The X-Y plane is the ground surface. The building is symmetrical about the coordinate planes, X-Z and Y-Z.

We select the X-Z plane as the input plane without losing the generalization. Here the angle of incidence is not used. Instead, its complement measured from the positive X-axis to the direction of the wave propagation is used. In this study, a seismic recording is input at the origin of the coordinate system, which is the control point. Only mass asymmetry is considered. The mass eccentricity is achieved by adjusting the mass density of the floor. The eccentricity of the building is large and mass center is located away from the geometrical center in the first quadrant. The eccentricity may be caused by the uneven mass distribution on the floor, such as equipment. The finite-element mesh, its architecture configuration and floor dimensions are given in Figure 1. The nodal points along the interface between soil and the building are given the soil properties, such as the density, Young's modulus and Poisson's ratio. In this study, the displacement of the building at the ground level is of most interest. The dynamic response of the building depends on the soil properties and on both the damping ratio and stiffness ratio of the soil and the building.

Governing equations

In this study, the unbounded soil is assumed to be a

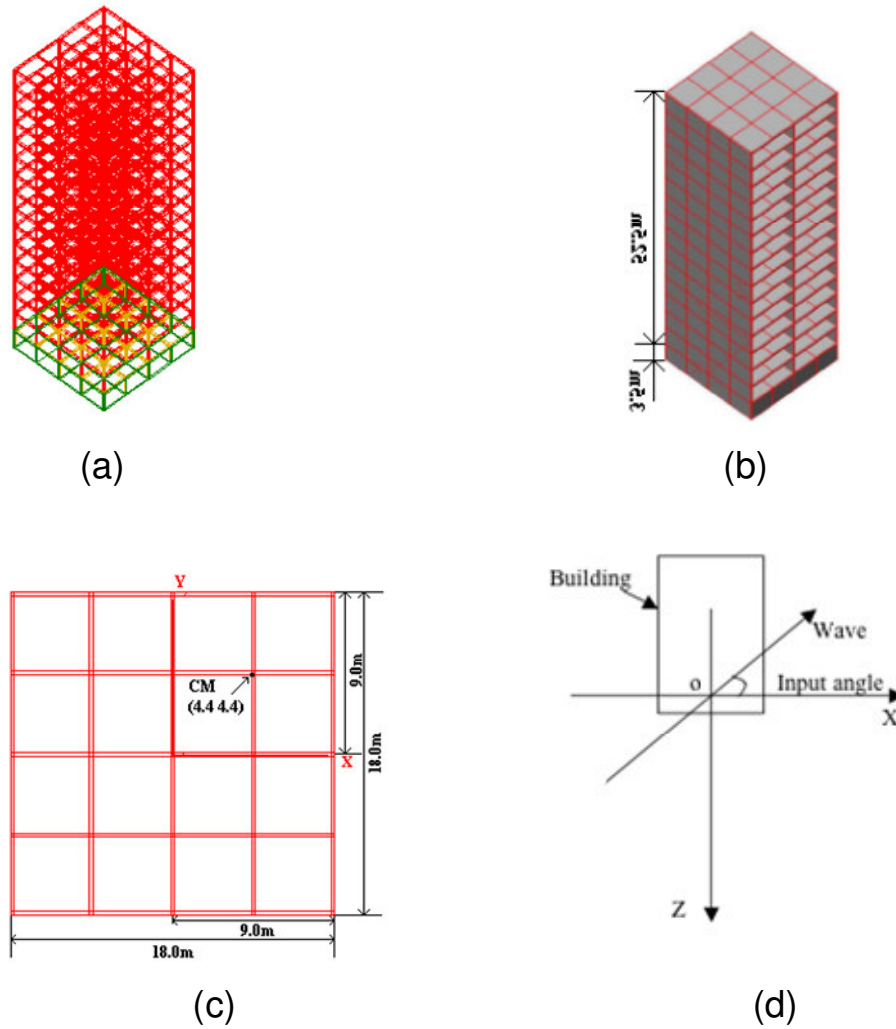


Figure 1. (a) The finite-element mesh model, (b) architecture model, (c) floor plan and (d) the coordinate system. The CM denotes the center of the mass, which located at (4.4, 4.4) in the first quadrant, with O as the coordinate center. The input angle is defined as the angle between the wave propagation direction and X-axis. The building is mass asymmetrical.

linear elastic solid and the equation of motion of the structure in the time domain can be expressed as (Wegner and Zhang, 2001),

$$\begin{bmatrix} \mathbf{M}_{zz} & \mathbf{M}_{zb} \\ \mathbf{M}_{bz} & \mathbf{M}_{bb} \end{bmatrix} \begin{Bmatrix} \ddot{\mathbf{u}}_z^t \\ \ddot{\mathbf{u}}_b^t \end{Bmatrix} + \begin{bmatrix} \mathbf{C}_{zz} & \mathbf{C}_{zb} \\ \mathbf{C}_{bz} & \mathbf{C}_{bb} \end{bmatrix} \begin{Bmatrix} \dot{\mathbf{u}}_z^t \\ \dot{\mathbf{u}}_b^t \end{Bmatrix} + \begin{bmatrix} \mathbf{K}_{zz} & \mathbf{K}_{zb} \\ \mathbf{K}_{bz} & \mathbf{K}_{bb} \end{bmatrix} \begin{Bmatrix} \mathbf{u}_z^t \\ \mathbf{u}_b^t \end{Bmatrix} = \begin{Bmatrix} \mathbf{0} \\ -\mathbf{r}_b^t(t) \end{Bmatrix} + \begin{Bmatrix} \mathbf{p}_s(t) \\ \mathbf{p}_b(t) \end{Bmatrix}, \quad (1)$$

where, \mathbf{M} is the mass matrix, \mathbf{K} is the stiffness matrix of the structure, \mathbf{C} is the viscous damping in the structure, \mathbf{u} , $\dot{\mathbf{u}}$, and $\ddot{\mathbf{u}}$ are the displacement, velocity and acceleration vectors, respectively, $\mathbf{r}_b(t)$ is the ground interaction force vector, and $\mathbf{p}(t)$ are the externally applied force vectors. In equation (1), the subscript b and s denote the nodes on the soil-structure interface and the nodes of the building, respectively, as shown in Figure 2. The superscript t represents the total motion of the structure. The

damping matrix \mathbf{C} is included here for completeness but is not considered in the numerical examples presented in this paper. The viscose damping of the building is not considered here. The building is assumed to be linear elastic. The ground interaction forces $\mathbf{r}_b(t)$ are given by the convolution integral (Zhang et al., 1999),

$$\mathbf{r}_b(t) = \int_0^t \mathbf{M}_{bb}^g(t-\tau) (\ddot{\mathbf{u}}_b^t(\tau) - \ddot{\mathbf{u}}_b^g(\tau)) d\tau \quad (2)$$

Where, $\mathbf{M}_{bb}^g(t)$ is the acceleration unit-impulse matrix and $\ddot{\mathbf{u}}_b^g(t)$ is the acceleration vector, at the nodes b (which will subsequently lie on the structure-soil interface) of the soil with excavation. Equation (2) can be used to

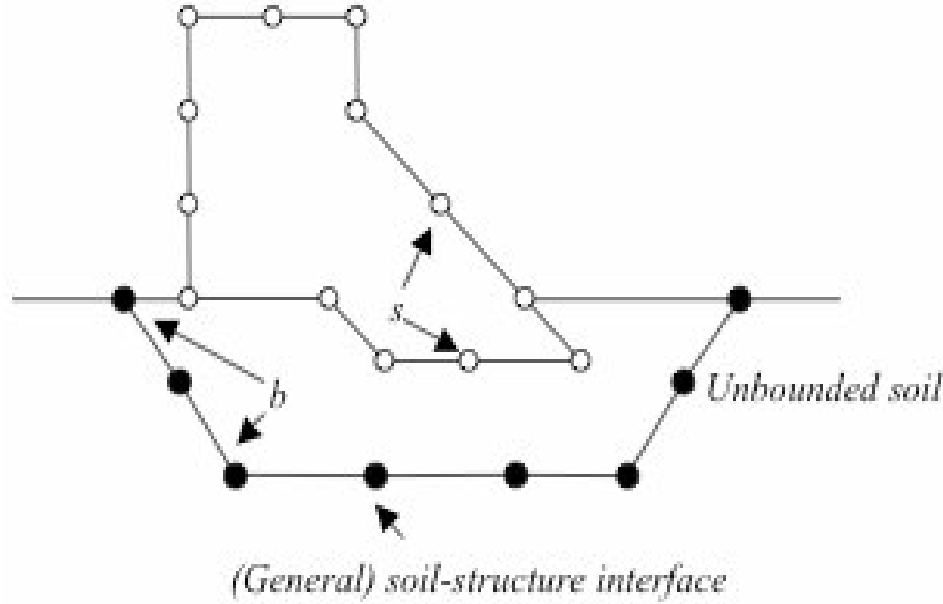


Figure 2. A soil-structure interaction system.

calculate a general wave pattern consisting of oblique body waves and surface waves. The ground motion $\ddot{\mathbf{u}}_b^g(t)$, depends on the excavation so that it is more convenient to replace this generalized scattered motion by the free-field motion $\ddot{\mathbf{u}}_b^f(t)$, which does not depend on the excavation, with the exception of the location of the nodes for which it is to be calculated, and can be determined by the free-field site analysis (Wolf, 1988; Chen, 1980). The free-field system results when the excavated part of the soil is added to the soil with excavation as indicated in Figure 2. For this special case, the structure consists of the excavated part of the soil only, and part of the integral on the right-hand side of equation (2) can be reformulated by considering the equation of motion as (Zhang et al., 1999),

$$\int_0^t \mathbf{M}_{bb}^g(t-\tau) \ddot{\mathbf{u}}_b^g(\tau) d\tau = \int_0^t \mathbf{M}_{bb}^f(t-\tau) \ddot{\mathbf{u}}_b^f(\tau) d\tau \quad (3)$$

Where \mathbf{M}_{bb}^f is the acceleration unit-impulse response matrix of the free-field site referred to the nodes at the soil-structure interface. To calculate the acceleration unit-impulse response matrix of the free field site, the excavated part of the soil is discretized by the finite-element method. Standard finite-element discretization of the excavated part of the soil results in the acceleration unit-impulse response matrix \mathbf{M}^e of the excavated soil, which is given by

$$\mathbf{M}^e = -\frac{1+2t\xi}{\omega^2} \mathbf{K}_e + \mathbf{M}_e \quad (4)$$

Where \mathbf{K}_e is the stiffness matrix of the excavated soil, \mathbf{M}_e is the mass matrix, ω is the circular frequency, $i = \sqrt{-1}$, and ξ is the hysteretic damping ratio of the excavated soil. The matrix \mathbf{M}^e can be decomposed into the sub matrices \mathbf{M}_{ii} , \mathbf{M}_{ib} and \mathbf{M}_{bb} . The subscript b refers to the nodes on the structure-soil interface, and the subscript i refers to the remaining nodes. Eliminating the degree of freedom at the i^{th} node leads to

$$\mathbf{M}_{bb}^e = \mathbf{M}_{bb} - \mathbf{M}_{bi} \mathbf{M}_{ii}^{-1} \mathbf{M}_{ib} \quad (5)$$

Where \mathbf{M}_{bb}^e is the acceleration unit-impulse response matrix of the excavated soil referred to the nodes b . Adding \mathbf{M}_{bb}^e to \mathbf{M}_{bb}^g results in the acceleration unit-impulse response matrix of the continuous soil \mathbf{M}_{bb}^f , discretized at the same nodes b , this subsequently lies on the structure-soil interface. That is,

$$\mathbf{M}_{bb}^f = \mathbf{M}_{bb}^e + \mathbf{M}_{bb}^g \quad (6)$$

Substituting equations (6) and (3) into equation (2) gives

$$\mathbf{r}_b(t) = \mathbf{r}_b^{(1)}(t) + \mathbf{r}_b^{(2)}(t) \quad (7)$$

Where,

$$\mathbf{r}_b^{(1)}(t) = \int_0^t \mathbf{M}_{bb}^g(t-\tau) (\ddot{\mathbf{u}}_b^g(\tau) - \ddot{\mathbf{u}}_b^f(\tau)) d\tau, \quad \mathbf{r}_b^{(2)}(t) = -\int_0^t \mathbf{M}_{bb}^e(t-\tau) \ddot{\mathbf{u}}_b^f(\tau) d\tau$$

The acceleration unit-impulse response matrix $\mathbf{M}_{bb}^g(t)$ is calculated using the scaled boundary finite-element method [13]. It can be decomposed as

Where \mathbf{K} is the static-stiffness matrix, \mathbf{C} is the matrix of dashpot coefficients at the circular frequency $\omega = 0$ of the unbounded soil, $\mathbf{H}(t)$ is the heaviside-step function, and $\mathbf{M}_f(t \rightarrow \infty) = 0$.

It may be shown that (Zhang et al., 1999)

$$\mathbf{r}_b^{(2)}(t) = -F^{-1} \left[\mathbf{M}_{bb}^e(\omega) \ddot{\mathbf{u}}_b^f(\omega) \right] \quad (8)$$

Where,

$F^{-1} \left[\mathbf{M}_{bb}^e(\omega) \ddot{\mathbf{u}}_b^f(\omega) \right]$ denotes the Inverse Fourier Transformation. The term enclosed in square brackets on the right-hand side of equation (8) is evaluated in the frequency domain and then transformed to the time domain as indicated. Substituting equation (7) into the equation of motion of the structure (1) enables the response of this structure-soil system to the incident seismic waves to be determined by a numerical integration scheme in the time domain (Zhang et al., 1999).

Nondimensional quantities

In this study, a non-dimensional scheme is used. The building height H and shear wave velocity in the soil are used as the characteristic length and velocity, respectively and the characteristic time is represented as $\hat{t} = \frac{H}{c_s}$.

$$\bar{t} = \frac{t}{\hat{t}}, \quad \bar{u} = \frac{u}{H}, \quad \bar{c}_p = \frac{c_p}{c_s}, \quad \bar{c}_s = 1, \quad \bar{E}_b = \frac{E_b}{E_s}, \quad \bar{E}_s = 1, \\ \bar{\rho}_b = \frac{\rho_b}{\rho_s}, \quad \bar{\rho}_s = 1,$$

are non-dimensional time, displacement, and P-wave velocity, S-wave velocity, Young's modulus and densities of the building and soil respectively. The storey height $H = 3.5$ m, shear wave velocity c_s equals 774 m/s, dilatational wave velocity c_p equals 1,341 m/s, density of the concrete building ρ_b equals 2,500 kg/m³, density of the soil equals 2,000 kg/m³, Young's modulus of the concrete building E_b equals 30 Gpa, Young's modulus of the soil E_s equals 30 Gpa. Henceforth, the superposed bars

will be omitted.

NUMERICAL RESULTS

In order to carry out the parametric study, a group of three buildings with one level basement model has been considered, as shown in Figure 1. The three buildings are of 5, 10 and 15 stories above ground. In this study, there are two types of loading applied to the buildings. In the first part of the study, only the externally applied force will be applied bi-directionally to the center of the mass at the ground level. The harmonic and earthquake loadings are adopted from (Lin and Tsai, 2008).

First, a sine wave is applied in the X-direction with the peak ground acceleration (PGA) equal to 0.80 g and another sine wave is applied in the Y-direction with PGA equal to 0.50 g, as shown in Figure 3. The loadings applied in X- and Y-direction are independent. Second, in order to facilitate a comparison study with the harmonic loading case, the recordings of the 1940 El Centro earthquake are amplified by 2.29 times. Thus, amplified earthquake recordings with PGA equal to 0.80 g in the NS component is applied in the X-direction and with PGA equal to 0.49 g in the EW component is applied in the Y-direction, as shown in Figure 4. For both cases, the SSL effect is not taken into account.

In the second part of the study, the amplified NS component of the 1940 El Centro earthquake recordings is used as the earthquake wave loading for studying the dynamic response of the two-way asymmetrical building with the inclusion of the soil-structure interaction effects. The loading point is chosen close to the origin of the coordinate system, which summarize the impinging forces acted by the incoming earthquakes. The input angle is measured from the positive X-axis in the direction of the wave propagation. The X-Z plane is the input plane for earthquake waves. The earthquake recordings is used directly as P, SH, and SV waves.

The response of buildings of different heights is compared and analyzed, including the soil-structure interaction. The relationships between the characteristics of the dynamic response of the buildings and the earthquake input are deducted. The loading is on the ground level of the building to simulate the impacting of the adjacent soil. These externally applied forces are of two-way asymmetrical to the building. The two different forces can best resemble the impact from the incoming earthquake waves from any direction. The displacement of the building roof will be calculated and compared. The rotation of the building due to the mass eccentricity is also studied.

Furthermore, these results are compared with the cases of symmetrical buildings under the same loading conditions. The effect of the coupling between the asymmetrical building and bi-directional asymmetrical loadings is revealed through the comparison with the results of sym-

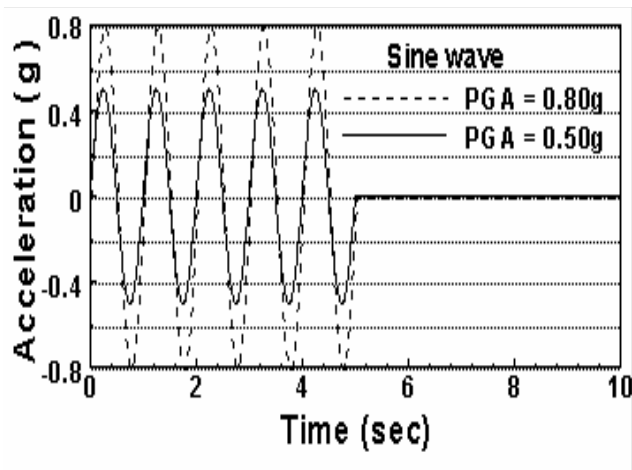


Figure 3. The sine waves with PGA equals to 0.80 g and 0.50 g.

symmetrical buildings.

Response to harmonic loading and 1940 El Centro earthquake loading

The response time histories of the building model subjected to the harmonic wave and earthquake loadings are obtained by using DSSIA-3D. Time histories of the center of the mass of the roof under the loading of sine wave with $PGA = 0.80\text{ g}$ applied in the X-direction and $PGA = 0.50\text{ g}$ applied in the Y-direction at the ground level. The variation of peak displacements in X, Y and Z-direction and rotation are shown in Figure 5 with the presence of earthquake loadings. The free vibration after the earthquake loading is ceased is not given here. The coupling between the characteristic of earthquake loadings and building vibration is the main focus. It is observed that the response of the asymmetrical building is close to a multiplication of harmonic waves, especially for a 5-story building. The response of the roof to the ground level loading is delayed by a few seconds.

Time histories of the center of the mass of the roof under the loading of El Centro earthquake with NS component applied in the X-direction and EW component applied in the Y-direction are shown in Figure 6. It can be seen that the response of the building is much more complex and random. In such a case, the damage to the structure would occur due to large displacement in one direction. From both cases, we can conclude that the rocking in the X-Z plane dominate the building's response characteristics. By comparing the three buildings with different heights, the mass effect on the response of the buildings decreases, especially when the building is subjected to a non-harmonic loading. Since the loading is ap-

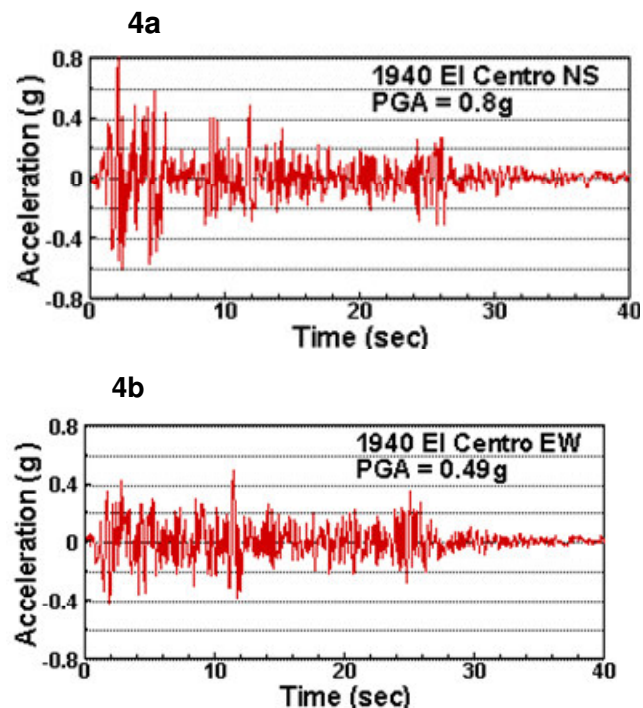
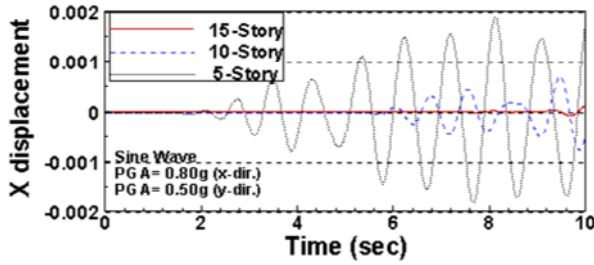


Figure 4. (a) 1940 El Centro Earthquake NS component applied in X direction (b) 1940 El Centro Earthquake EW component applied in Y direction.

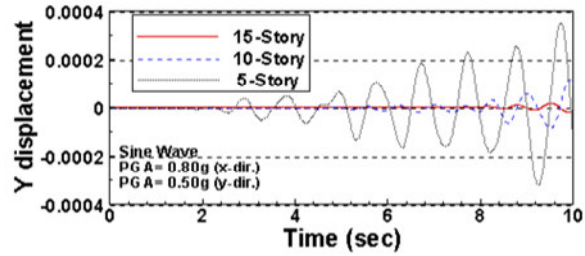
plied at the ground level, the higher the building, the later the roof will start reacting. Overall, the low to medium sized building reacts to the earthquake loading most dramatically.

Response to 1940 El Centro earthquake loading with SSI effect

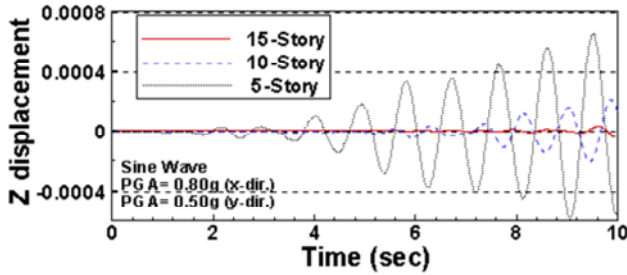
In the second part of this study, the responses of the same asymmetrical buildings subjected to an earthquake loading with SSI effect are obtained by using DSSIA-3D. The incoming earthquake waves are of different types, such as P waves and shear waves: SH and SV waves. The input angle for P waves varies from 30 to 90 degrees. The wave input plane is the XZ plane and with X parallel to the ground. Non-dimensional displacement of the center of mass of the asymmetrical building subjected to 1940 El Centro earthquake loadings in different wave types at different input angles, shown in Figure 7(a) - (e) are P waves with input angles of 30, 60° and vertically, SH waves with an input angle of 60°, SV waves with an input angle of 60°. It is observed that the displacement in the X direction decreases as the input angle increases. The dominant response shifts from X direction to vertical direction, as well as its magnitude. This shift is corresponding to the decreasing strength of the horizontal compo-



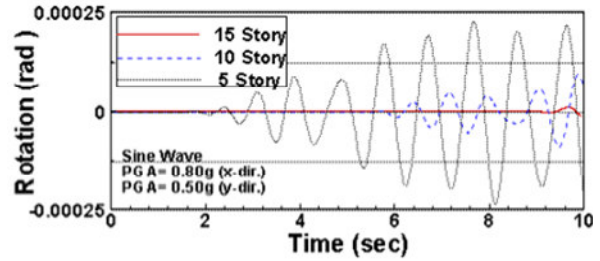
5(a)



5(b)



5(c)



5(d)

Figure 5. Time histories of the center of the mass of the roof under the loading of sine wave with PGA = 0.80 g applied in the X-direction and PGA = 0.50 g applied in the Y-direction at the ground level: 5(a) displacement in X-direction; 5(b) displacement in Y-direction; 5(c) displacement in Z-direction; 5(d) rotation.

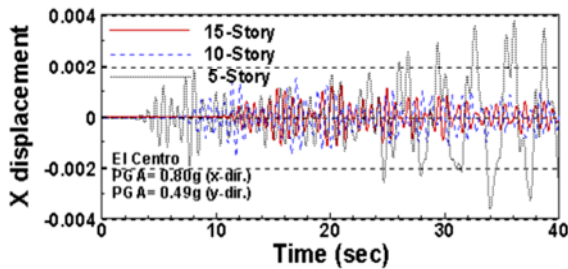


Figure 6(a)

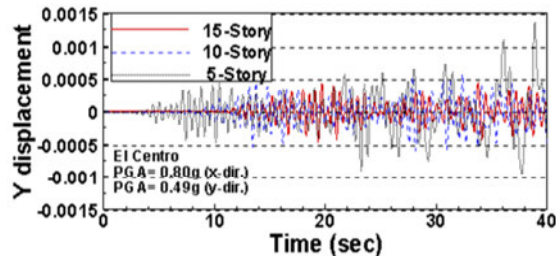


Figure 6(b)

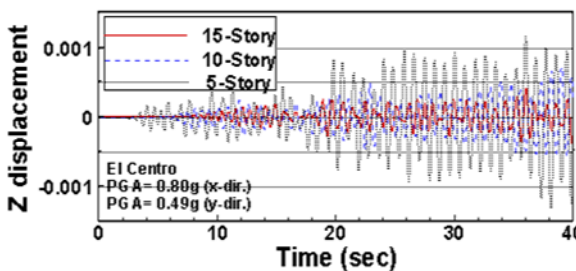


Figure 6(c)

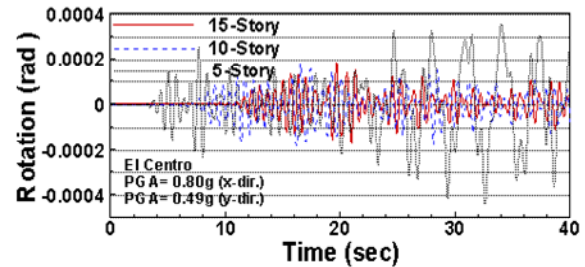


Figure 6(d)

Figure 6. Time histories of the center of the mass of the roof for the 15-story asymmetrical building under the loading of El Centro earthquake with NS component applied in the X-direction and EW component applied in the Y-direction at the ground level: 6(a) displacement in X-direction; 6(b) displacement in Y-direction; 6(c) displacement in Z-direction; 6(d) rotation.

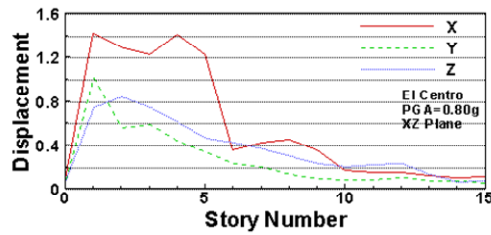


Figure 7(a)

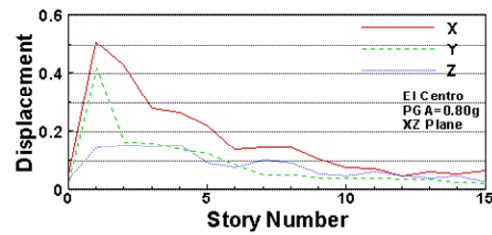


Figure 7(b)

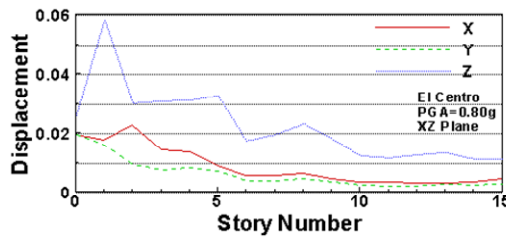


Figure 7(c)

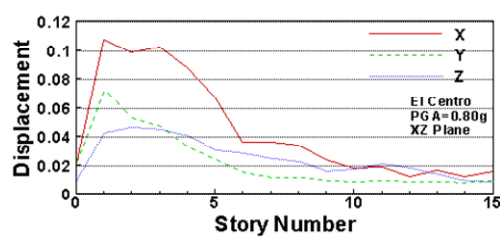


Figure 7(d)

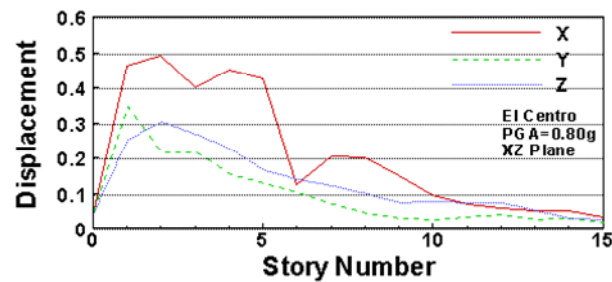


Figure 7(e)

Figure 7. Non-dimensional displacement ($\times 10^2$) of the center of mass of the 15-story asymmetrical building subject to 1940 El Centro earthquake loadings in different wave types at different input angles: 7(a) P wave with an input angle of 30° ; 7(b) P wave with an input angle of 60° ; 7(c) P wave input vertically; 7(d) SH wave with an input angle of 60° ; 7(e) SV wave with an input angle of 60° .

ment of wave motion as the input angle increases from 30° to 90° . This also implies that the damage caused by P waves becomes less dominant for buildings located at the closer distance from the epicenter. The shear wave will be the dominant factor for causing building damages at locations closer to the epicenter. For instance, if the depth of the fault is D and the distance from epicenter is L , then for the input angle of 60° , the relationship between L and D can be approximately represented as $L = 0.58D$. This formula means the building is close to the epicenter. For the same input angle of 60° and to the same building, we can observe that the SV wave results in the same magnitude of displacement in the dominant X direction as for the P wave. This is explained by the concentration of kinetic energy of soil particles in the input X-Z plane for P waves and SV waves. However, for SH waves, the soil particles are vibrating in the perpendicular direction to the X-Z plane. The dominant displacement of the lower part of the building caused by the SV wave are about 5 times

larger than that by the SH wave under the same conditions for the displacement in the X direction.

From the simulated results for both P waves and shear waves, at the lower level of the building, the large peak displacement is observed during the same period of the earthquake event. In such a short period time, the building is subjected to a strong ground motion. The building is under the condition of forced vibration. Large displacement and deformation of the lower level of the building are the consequence of the forced vibration. After a major earthquake, the collapse at the lower level of the building is often observed.

The building height factor

Subject to the same waves and angles of input, the response characteristics of the different heights of buildings are compared. This study corresponds to the scenario where different height of building located in the same

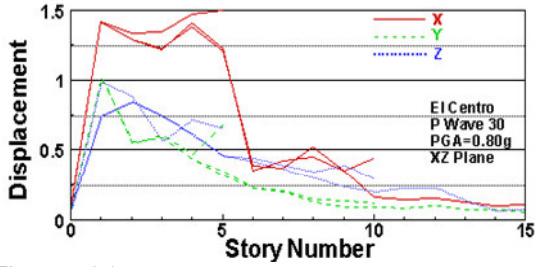


Figure 8(a)

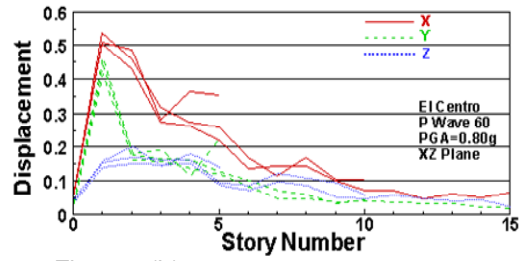


Figure 8(b)

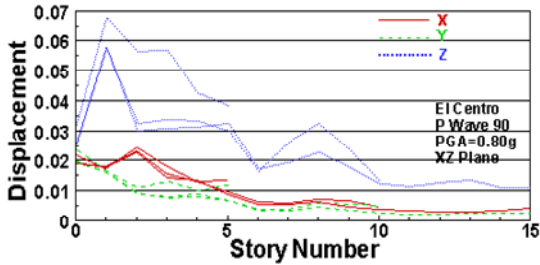


Figure 8 (c)

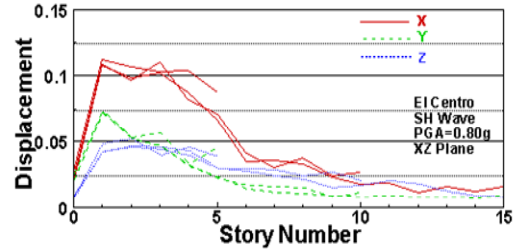


Figure 8(d)

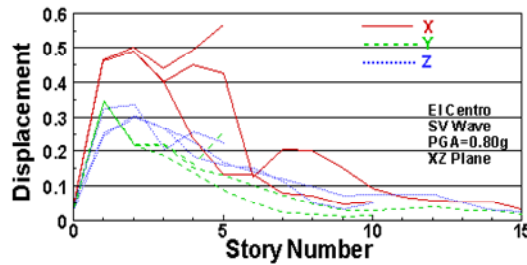


Figure 8(e)

Figure 8. Non-dimensional displacement ($\times 10^2$) of the center of mass of the asymmetrical building with different height subject to 1940 El Centro earthquake loadings in different wave types at different input angles: 8(a) P wave with input angle of 30° ; 8(b) P wave with input angle of 60° ; 8(c) P wave input vertically; 8(d) SH wave with input angle of 60° ; 8(e) SV wave with input angle of 60° .

during a major earthquake. With the only difference of building height as the variable, the different response to the same earthquake can be examined. It is observed from Figure 8, the dominant displacement is in the X-direction for P waves for input angles are less than 60° , or for the same strength of P waves at the further distance from the epic center. The dominant displacement shifts to Z-direction, when P waves propagate vertically towards the building compared with the displacement in other directions.

The largest displacement will result for cases of input P waves propagating close to surface. The same conclusion can be drawn for the shear wave cases. Especially, for shorter buildings, such as the 5-level building, the peak displacement of the roof is larger than other taller buildings. Also, the largest displacement usually can be found around the ground level. The low inertia of the low level building characterizes the large displacement of the whole building which is contrast to the small displacement of the roof for taller buildings.

The comparison between asymmetrical and symmetrical buildings with SSI effect

In order to identify the significant influence from the mass eccentricity toward the building's response during earthquakes, the symmetrical building with even mass distribution is studied under the same bi-directional asymmetrical loading conditions. The mass eccentricity is the only influence factor under examined here. A 15-story building is used for this purpose without losing the generalization. For comparison, both nodal points in the symmetrical building and asymmetrical building are chosen with the same coordinates. Under the same loading conditions, the asymmetrical building has larger displacements than the symmetrical building overall, especially in the X and Z direction. The uneven mass distribution is the only factor that contributes to the larger displacement in the asymmetrical building. For different types of waves, the P and SV waves result in a much stronger response from the building than the SH waves do, as shown in Figure 9

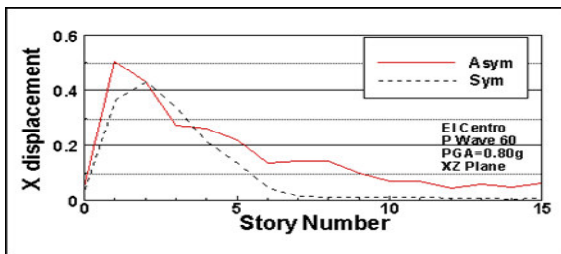


Figure 9(a)

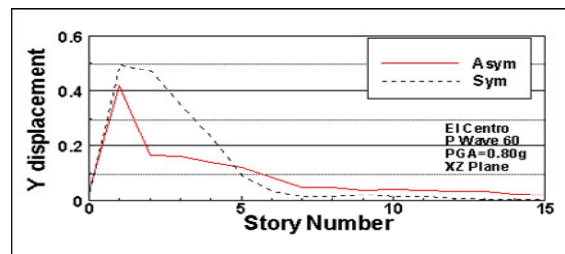


Figure 9(b)

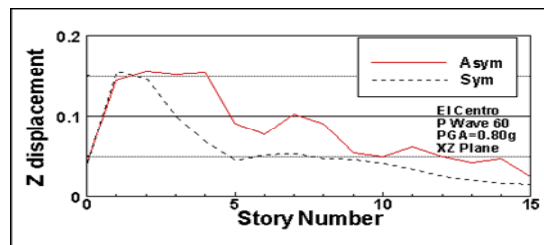


Figure 9(c)

Figure 9. Non-dimensional displacement ($\times 10^2$) of the center of mass of the 15-story sym-metrical building subject to 1940 El Centro earthquake loadings in P wave with input angle of 60: 9(a) X displacement; 9(b) Y displacement; 9(c) Z displacement.

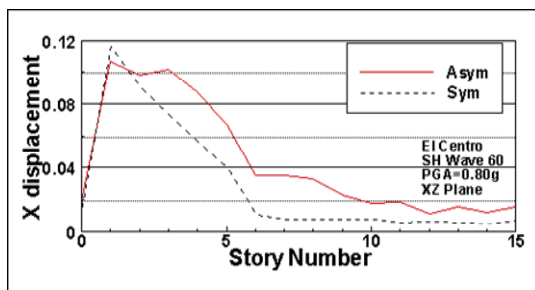


Figure 10(a)

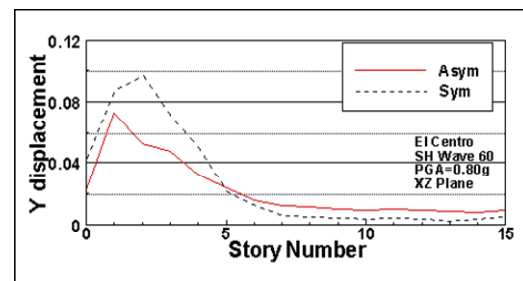


Figure 10(b)

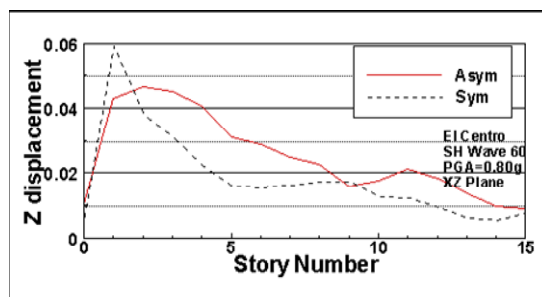


Figure 10(c)

Figure 10. Non-dimensional displacement ($\times 10^2$) of the center of mass of the 15-story symmetrical building subject to 1940 El Centro earthquake loadings in SH wave with input angle of 60: 10(a) X displacement; 10(b) Y displacement; 10(c) Z displacement

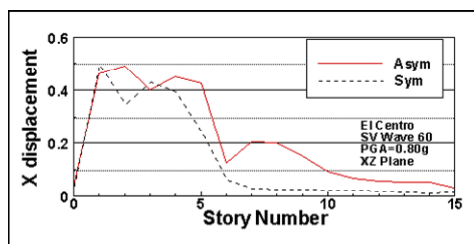


Figure 11(a)

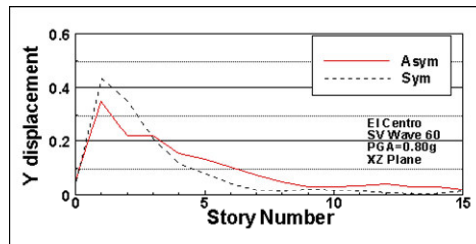


Figure 11(b)

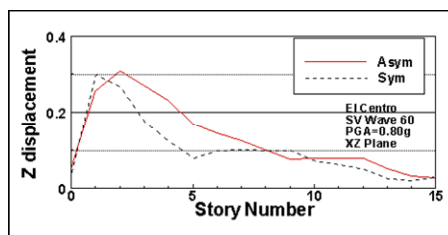


Figure 11(c)

Figure 11. Non-dimensional displacement ($\times 10^2$) of the center of mass of the 15-story symmetrical building subject to 1940 El Centro earthquake loadings in SV wave with input angle of 60: 11(a) X displacement; 11(b) Y displacement; 11(c) Z displacement.

- 11. For example, the displacement in the X and Y direction caused by P and SV waves is about 5 times larger than those caused by SH waves. This is consistent with the observation made earlier from the symmetrical building cases.

Conclusions

The magnitude of the dominant earthquake component coupled with the eccentric character of the building determined the building's response characteristics of the buildings. The lower to medium sized buildings incurred the most impact from the earthquakes. The mass effect is not a major influential factor for tall buildings. The asymmetrical building coupled with the two-way asymmetrical earthquake loadings will amplify the damages to the structure compared with symmetrical buildings. These results are consistent with the field observation after major earthquakes.

REFERENCES

- Ben JS, Shiojiri H (2000). A method for three dimensional interaction analysis of pile-soil system in time domain. *Trans Jpn. Soc. Comput. Eng. Sci.*
- Tzong TJ, Penzien J (1983). Hybrid modeling of soil-structure interaction in layered media. Report no. UCB/EERC-83/22. Berkeley: EERC, Univ. of California.
- Chen CH, Penzien J (1986). Dynamic modeling of axisymmetric foundation. *Earthquake Eng Struct Dyn* 14:823-40.
- Luco JE (1974). Impedance functions for a rigid foundation on a layered medium. *Nuclear Eng.* 31:204-17.
- Wong HL, Luco JE (1976). Dynamic response of a rigid foundation of arbitrary shape. *Earthquake Eng. Struct. Dyn.* 4:579-87.
- Wong HL, Luco JE (1985). Tables of impedance functions for square foundations on layered media. *Soil Dyn. Earthquake Eng.* 4:64-81.
- Liou GS (1989). Analytical solutions for soil-structure interaction in layered media. *Earthquake Eng. Struct. Dyn.* 18:667-86.
- Lysmer J, Kuhlemeyer RL (1969). Finite dynamic model for infinite media. *J Eng Mech. Div. ASCE.* 95:859-77.
- White W, Valliappan S, Lee IK (1969). Unified boundary for finite dynamic model. *J. Eng. Mech. Div. ASCE.* 103:160-74.
- Werkle H (1986). Dynamic finite element analysis of three dimensional soil models with transmitting element. *Earthquake Eng. Struct. Dyn.* 14: 41-60.
- Tassoulas JL (1983). Elements for the numerical analysis of wave motion in layered media. *Int. J. Numer. Methods Engrg.* 19:1005-32.
- Song CM, Wolf JP (1998). The scaled boundary finite-element method: analytical solution in frequency domain. *Comput. Methods Appl. Mech. Engrg.* 164:249-64.
- Song CM, Wolf JP (2000). The scaled boundary finite-element method - a primer: solution procedures. *Comput. Struct.* 78:211-225.
- Chopra AK (1995). *Dynamics of structures: theory and applications to earthquake engineering.* Englewood Cliffs, NJ: Prentice-Hall.
- Kan CL, Chopra AK (1977). Elastic earthquake analysis of torsionally coupled multi-story buildings. *Earthquake Eng. Struct. Dyn.* 5:395-412.
- Kan CL, Chopra AK (1981). Simple model for earthquake response studies of torsionally coupled buildings. *Engng Mech. Div. ASCE.* 107:935-51.
- Hejal R, Chopra AK (1989). Earthquake analysis of a class of torsionally coupled buildings. *Earthquake Eng. Struct. Dyn.* 18:305-23.
- Chandler AM, Duna XN (1991). Evaluation of factors influencing the inelastic seismic performance of torsionally asymmetric building. *Earthquake Eng. Struct. Dyn.* 20:87-95.
- Shakib H, Datta TK (1993). Inelastic response of torsionally coupled system to an ensemble of non-stationary ground motion. *Engng. Struct.* 15:13-20.
- Paulay T (1997). Seismic torsional effects on ductile structural wall systems. *Earthquake Engrg.* 1:721-45.
- Myslimaj B, Tso WK (2002). A strength distribution criterion for mini-

- mizing torsional response of asymmetric wall-type systems. *Earthquake Eng. Struct. Dyn.* 31:99–120.
- Shakib H, Touhidi RZ (2002). Evaluation of accidental eccentricity in buildings due to rotational components of earthquake. *Earthquake Eng.* 6:431–45.
- Armando B, Luis E (2007). Influence of dynamic soil–structure interaction on the nonlinear response and seismic reliability of multi-storey systems. *Earthquake Eng. Struct. Dyn.* 36:327–346.
- Shakib H, Fuladgar A (2004). Dynamic soil–structure interaction effects on the seismic response of asymmetric buildings. *Soil Dyn Earthquake Eng.* 24:379–388.
- Zhang X, Wegner JL, Haddow JB (1999). Three dimensional soil–structure–wave interaction analysis in time domain. *Earthquake Eng Struct Dynam.* 36:1501–24.
- Wegner JL, Zhang X (2001). Free vibration analysis of a three-dimensional soil–structure system. *Earthquake Eng. Struct. Dynam.* 30:43–57.
- Wegner JL, Yao MM, Zhang X (2005). Dynamic wave–soil–structure interaction analysis in the time domain. *Comput. Struct.* 83:2206–2214.
- Wolf JP (1988). *Soil structure in the time domain*. Englewood Cliffs, NJ: Prentice-Hall.
- Chen J (1980). *Analysis of local variations in free field seismic ground motion*. Ph.D. Dissertation, University of California, Berkeley.
- Lin JL, Tsai KC (2008). Seismic analysis of two-way asymmetric building systems under bi-directional seismic ground motions. *Earthquake Eng. Struct. Dynam.* 37:305–328.

Nomenclature	
DSSIA	Dynamic soil-structure interaction analysis
SBFEM	Scaled boundary finite-element method
BEM	Boundary element method
FEM	Finite-element method
SSI	Soil-structure interaction
PGA	Peak ground acceleration
M	Mass matrix
K	Stiffness matrix
u	Displacement vector
\dot{u}	Velocity vectors
\ddot{u}	Acceleration vectors
$r_b(t)$	Ground interaction force vector
$p(t)$	Externally applied force vector
C	Damping matrix
$M_{bb}^g(t)$	Acceleration unit-impulse matrix
$\ddot{u}_b^g(t)$	Acceleration vector, at the nodes b
$\ddot{u}_b^g(t)$	Ground motion
$\ddot{u}_b^f(t)$	Free-field motion
M_{bb}^f	Acceleration unit-impulse response matrix of the free field site
M^e	Acceleration unit-impulse response matrix of the excavated soil
M_{bb}^e	Acceleration unit-impulse response matrix of the excavated soil
K_e	Stiffness matrix of the excavated soil
M_e	Mass matrix of the excavated soil
M_{ii}, M_{ib}, M_{bb}	Submatrices of M_e
ξ	The hysteretic damping ratio of the excavated soil
ω	Circular frequency
c_s	Shear wave velocity
c_p	Dilatational wave velocity
ρ_s	The density of the soil
ρ_b	Density of the concrete building
E_b	Young's modulus of the concrete building
E_s	Young's modulus of the soil
Superscripts	
T	Total motion of the structure
g	Unbounded ground soil with excavation
F	Free-field site
e	Excavated soil
Subscripts	
b	Nodes of the building
s	Nodes of the soil structure interface
e	Excavated soil
i	Refers to the remaining nodes